Rare Metal Materials and Engineering
Volume 51, Issue 1, January 2022
Available online at www.rmme.ac.cn

Science Press

Cite this article as: Zhao Fei, Liu Zijing, Ma Lifeng, et al. EBSD Analysis of Microstructure of EQ309L Stainless Steel After Band Electrode Submerged Arc Overlay Welding[J]. Rare Metal Materials and Engineering, 2022, 51(01): 98-105.

ARTICLE

EBSD Analysis of Microstructure of EQ309L Stainless Steel After Band Electrode Submerged Arc Overlay Welding

Zhao Fei[1], Liu Zijing[1], Ma Lifeng[2], Zhao Guanghui[2]

[1] School of Materials Science and Engineering, Taiyuan University of Science and Technology, Taiyuan 030024, China; [2] Coordinative Innovation Center of Taiyuan Heavy Machinery Equipment, Taiyuan 030024, China

Abstract: Band electrode submerged arc overlay welding was used to weld welding strip of EQ309L stainless steel on the surface of Q345R matrix. The microstructure of EQ309L side, Q345R side, and their interfaces were observed by electron backscattered diffraction (EBSD) technique. Results show that most grains in Q345R matrix are seriously distorted, and the banded grains along the original rolling direction can be clearly observed. The average grain size of Q345R matrix is 30~40 μm in the overheated coarse-grain region, and the grain coarsening is not severe. The average grain size of the fine-grain region is 10~20 μm in the Q345R matrix. The transition zone is 35~40 μm away from the fusion line of Q345R matrix, and it has body-centered cubic (bcc) structure. The EQ309L layer has coarse grains, showing the microstructure of columnar crystal with obvious <100> texture.

Key words: microstructure; band electrode submerged arc overlay welding; EQ309L; EBSD

Many thick-wall pressure vessels, such as petrochemical vessels and nuclear power equipment, can be operated under high temperature and high pressure and corroded by the medium. Generally, the stainless steel cladding is required on the inner wall of the vessels[1-3]. According to the working temperature, corrosion characteristics, and crack resistance factors of the corrosive medium, the commonly used stainless steel cladding includes EQ309L/308L, EQ309L/316L, and EQ309L/347. The first layer of EQ309L stainless steel is mainly applied to form a high toughness transition layer between the base metal and the surface layer to prevent the surface cracks of the base metal. Meanwhile, the reduction of alloy elements (Cr,Ni) caused by the dilution of base material is usually solved through carefully controlling the alloy composition of the welded cladding. The surface layers of 308L, 316L, and 347 stainless steels mainly play an important role in the corrosion resistance[4,5].

Compared with the electrode arc welding and molten electrode gas shielded welding, the band electrode submerged arc overlay welding has many advantages, such as high deposition efficiency, good welding quality, low dilution rate, and smooth surface of the weld bead. It can process the material without mechanical processing and hardly produce welding defects at the joints between the weld and the base metal[6,7]. It is an optimized choice for surface welding on the inner surface of a pressure vessel.

The connection between the base material and the austenitic stainless steel is mainly completed by fusion welding. Due to the special heat effect of welding and the formation of the molten pool, the fusion zone at the joint of base metal and the weld pool is regarded as the weakest part of the welded joint, i.e., most damaged regions in the welded structure originate from the welding fusion zone[8-10]. Based on the structural analysis, the weld pool is a solid structure with columnar crystals or dendrites, and the base material, which is only affected by heat, is a solid structure with different grain sizes. The welding fusion zone is the interface between the solidified structure and the solid structure of the base metal[11-14]. Therefore, it is necessary to study the grain growth process and grain transformation at high temperatures, and the orientation relationship between the solidified grains and the grains of solid base metal near the fusion zone. It is of great

Received date: June 25, 2021
Foundation item: Key Research and Development (R&D) Projects of Shanxi Province (201903D121054); Innovation Project of Colleges and Universities in Shanxi Province (2019L0621); Science and Technology Major Project of Shanxi Province (20181101015)
Corresponding author: Zhao Fei, Ph. D., Associate Professor, School of Materials Science and Engineering, Taiyuan University of Science and Technology, Taiyuan 030024, P. R. China, E-mail: 2012020@tyust.edu.cn

significance to investigate the failure laws and performance changes of welded joints[15-17].

The optical microscope (OM) and X-ray diffraction (XRD) methods were used to investigate the microstructure characteristics of the region near the fusion zone of Fe-Si alloys and in the heat-affected zone of the base metal. It is found that the welded grains grow from the epitaxial nucleation of the grains in the heat-affected zone of base metal. Furthermore, based on the anisotropy of welded grains, it is also found that the competitive growth of grains is not only affected by the epitaxial nucleation, but also closely related to the shape of the weld pool. In addition, the grain growth and grain boundary migration characteristics of the crystallization of molten pool can be obtained by mathematical models[18,19].

In this research, EQ309L stainless steel strip was processed by band electrode submerged arc overlay welding method on the vessel surface of Q345R base metal. The weld pool, the crystallization of weld metal near the liquid-solid interface, the grain growth, the structure evolution laws, and orientation evolution characteristics were investigated to provide a theoretical basis for the formation mechanism of the welding fusion zone.

1 Experiment

The experiment materials were produced by Taiyuan Iron and Steel (Group) Co., Ltd (Taiyuan, China), and their sizes and chemical composition are displayed in Table 1 and Table 2, respectively.

The welding process produces harmful impurities on the surface, such as rust, oil, and moisture, which should be eliminated for a non-defect surface with no delamination, crack, or inclusion. Before the surface welding of the transition layer, the specimen was pre-heated to above 100 °C. Because the large temperature difference is ascribed to the hot cracks before and during welding, the pre-heating process can control the moisture content of the specimen. The belt pole surface welding method was used, EQ309L welding tape was selected as the transition layer, and the welding distance of transition layer was 3 mm. The matching flux SJ304D and calcium silicate type neutral sintered flux were selected. The main composition is SiO_2, TiO_2, CaO, MgO, Al_2O_3, MnO, and CaF_2. The flux was sintered at 300~350 °C for 2 h before use. The surface of the transition layer and the overall surface layer were subjected to penetrant flaw tests after overlay welding, and the I grade was achieved. The experiment parameters and schematic diagram of band electrode submerged arc overlay welding are shown in Table 3 and Fig. 1, respectively. The surface of the entire overlay welding layers was flat and smooth; the depression between the adjacent weld beads was less than 1 mm; the roughness of the welded joint was less than 1 mm.

After band electrode submerged arc overlay welding, the specimens were cut along the rolling direction (RD) - normal direction (ND) surface of Q345R base metal by wire-electrode cutting. The original morphologies are shown in Fig. 2, indicating that the size of equiaxial grain is fine. Standard metallographic procedures were conducted to polish the bonding surface area of EQ309L and Q345R stainless steels. Then, a Buehler vibration machine was used to polish the specimen for 2 h to ensure that every residual surface deformation was removed. The polishing medium of the vibration mill was non-crystallized colloidal silica polishing suspension. Finally, the microstructure characteristics were analyzed by electron backscattered diffraction (EBSD).

According to the metallographic specimen preparation, the specimen was polished and then corroded with 4vol% nitric acid alcohol, and then the microstructure and indentation morphology were observed using a Leica DM2700M metallurgical microscope. Zeiss scanning electron microscopy (SEM) coupled with energy dispersive spectroscopy (EDS) was used to analyze the diffusion behavior of elements in the heat-affected zone. The Vickers microhardness tester (HV-120) was used to analyze the microhardness variation from the welded zone to the base metal based on 40 dots with the interval of 0.1 mm. Subsequently, 35 points with the interval of 0.2 mm were selected. Each point had a load of 0.2 kg, and the pressure holding time was 10 s.

Table 1 Size of experiment materials

Material	Application	Thickness/mm	Size	Mass/kg
Q345R	Base metal	30	200 mm×400 mm	1
EQ309L	Strip	0.5	60 mm×0.5 mm	3
SJ304D	Flux	-	-	5

Table 2 Chemical composition of experiment materials (wt%)

Material	C	Si	Mn	P	S	Ni	Cr	Mo	Cu	Co	Ti	N	Fe
Q345R	0.160	-	1.460	0.012	0.004	-	-	-	-	-	0.150	-	Bal.
EQ309L	0.012	0.370	1.630	0.013	0.003	13.200	24.000	0.060	0.030	0.040	0.007	0.040	Bal.

Table 3 Experiment parameters of band electrode submerged arc overlay welding

Welding region	Pre-heating temperature/°C	Size	Welding current/A	Welding voltage/V	Line energy/kJ·cm^{-1}	Welding speed/cm·min^{-1}
EQ309L layer	100~200	60 mm×0.5 mm	750~850	25~29	≤82.2	15~20

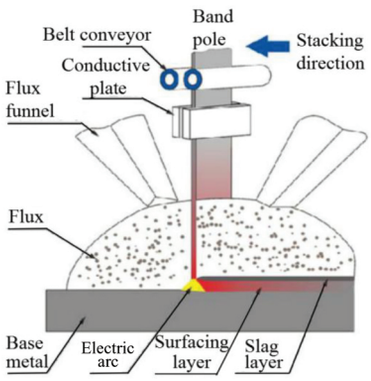

Fig.1 Schematic diagram of band electrode submerged arc overlay welding

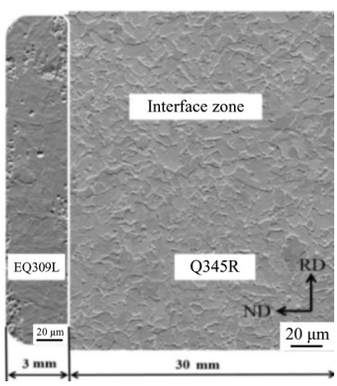

Fig.2 Morphologies of EQ309L and Q345R stainless steels

2 Results

2.1 Interface structure analysis

Two locations (Area 1 and Area 2) in the interface area were selected for the EBSD characterization, as shown in Fig. 3. The left side is the overlay welding layer of EQ309L stainless steel, the right side is the base metal of Q345R stainless steel, and the middle area represents the transition layer between different stainless steels. It can be seen from the Fig. 3 that the Q345R base metal basically occupies the blue recrystallized area, the EQ309L overlay welding layer occupies the yellow sub-crystalline area, and the transition layer is the red deformed area. The EQ309L overlay welding layer has coarse grains and columnar crystal morphology.

During the welding process, the structure and performance of the base metal near the welding area can be affected by the welding thermal cycle. The heating effect on the base material changes, leading to different structures in the welding heat-affected zone. The welding heat-affected zone of different stain steels can be generally divided into different parts: fusion line, coarse-grain zone in overheating area, fine-grain zone in normalizing area, and tempering zone. The coarse-grain region is the main reason for weakened performance and quality of welded joints. As shown in the overheated coarse-grain region in Fig.3, the average grain size is 30~40 μm, and the grain coarsening is not severe. The fine-grain area in the right side has the average grain size of 10~20 μm.

In the interface area, three locations (Area 1, Area 2, and Area 3) were selected for EBSD characterization, as shown in Fig. 4. The left side is the overlay welding layer of EQ309L stainless steel, the right side is the base metal of Q345R stainless steel, and the middle area represents the transition layer, which is similar to the structure in Fig. 3. The misorientation angle in Fig. 4 is 1°~7.5°. Q345R base metal basically occupies the blue recrystallized area, the EQ309L overlay welding layer occupies the yellow sub-crystalline area, and the transition layer is the red deformed area.

According to Fig. 4, it is obvious that the grains in heat-affected zone of the base metal on both sides of the fusion zone connect to the welded columnar crystals, indicating that the grain boundaries are continuous at the fusion zone. Thus, the unmelted metal in heat-affected zone of base metal near the fusion zone acts as the mold wall of the molten pool, because the overlay welding metal EQ309L is mainly composed of face-centered cubic (fcc) austenite and the Q345R base metal is mainly composed of body-centered cubic (bcc) ferrite. The fusion zone between the overlay welding metal EQ309L and the base metal Q345R is obvious. The transition zone locates at the area of 35~40 μm away from the fusion line on the substrate side extending to the overlay welding zone, where the stirring resistance of the molten pool is relatively large. The content of alloying elements Cr and Ni is significantly decreased in the overlay welding layer of EQ309L stainless steel due to the dilution by Q345R base metal. This area has a bcc structure due to the dilution effect of the austenitic ribbon. The ferrite content in the transition zone is relatively high, and the solidification modes are ferrite and austenite modes, resulting in the clear grain boundaries between the transition zone and the overlay welding layer.

2.2 EQ309L layer structure analysis

Fig. 5 shows IPFs, reverse pole figures, and pole figures of the overlay welding layers of EQ309L stainless steel at three locations (Area 1, Area 2, and Area 3) near the overlay welding interface. The <100> texture can be observed from the pole figures and the reverse pole figures of different positions. During the overlay welding process of EQ309L stainless steel, the composition and the crystalline structure of the overlay welding layer are both different from those of the Q345R base metal. In this case, the epitaxial growth cannot proceed, and grains with different structures are nucleated at the melting boundary.

Nelson[20] investigated the base metal and the welded metal with different grain structures at solidification temperature. The nucleation of solid welded metal appears in the heterogeneous region of semi-molten base metal at the melting boundary. Due to the heterogeneous nucleation at the melting boundary, the grain orientation between the base metal and the welded metal is random. The orientation of the welded metal and the base metal is either consistent or not, indicating that the grains of welded metal can achieve a certain atomic layer which is parallel to the specific atomic layer in the base metal.

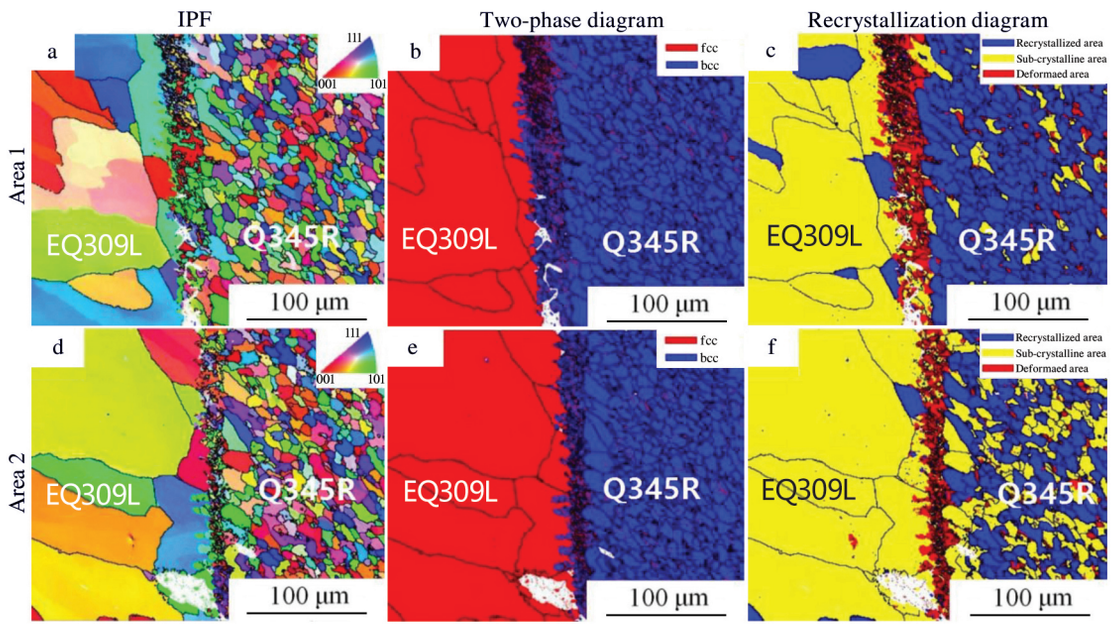

Fig.3 EBSD characterization diagrams at low magnification of Area 1 (a~c) and Area 2 (d~f) of interface: (a, d) inverse pole figures (IPFs), (b, e) two-phase diagrams, and (c, f) recrystallization diagrams

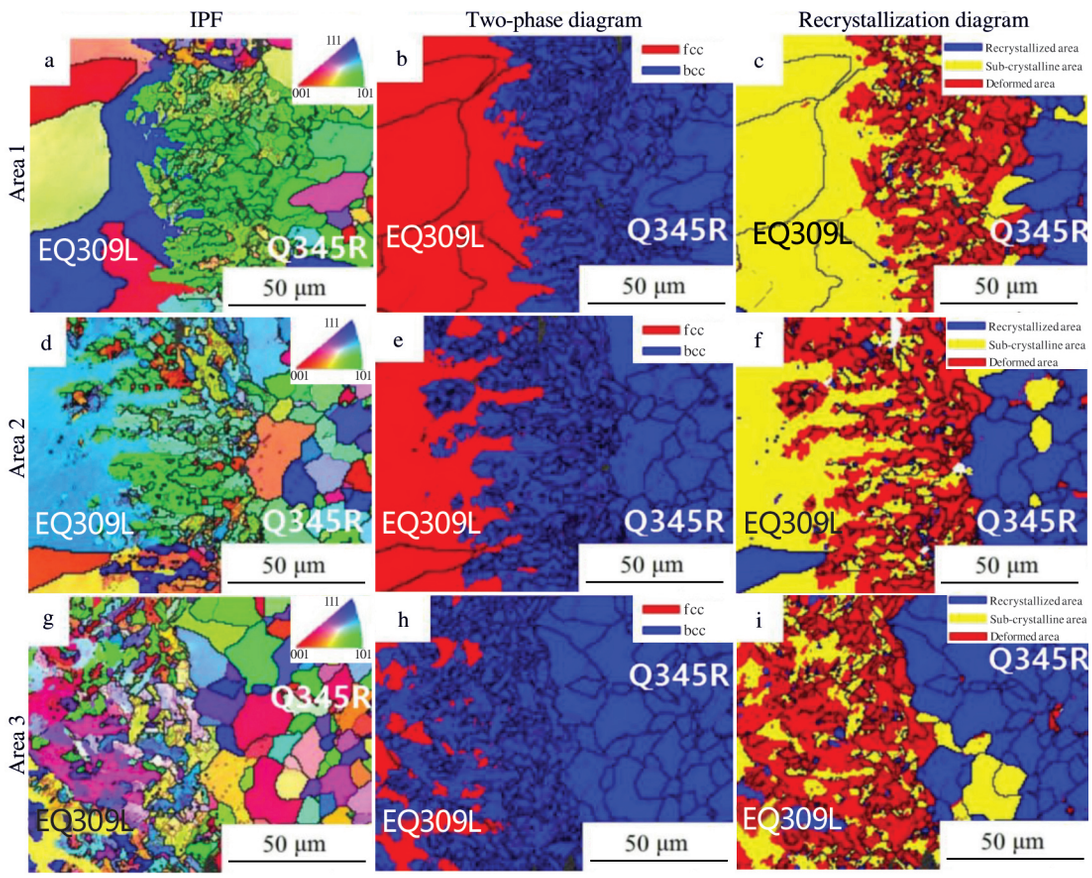

Fig.4 EBSD characterization diagrams at high magnification of Area 1 (a~c), Area 2 (d~f), and Area 3 (g~i) of interface: (a, d, g) IPFs, (b, e, h) two-phase diagrams, and (c, f, i) recrystallization diagrams

When the base metal and welded metal have different grain structures, the structure of grains near the melting boundary depends on the nucleation of new grains, whereas the structure of grains outside the melting boundary is mainly

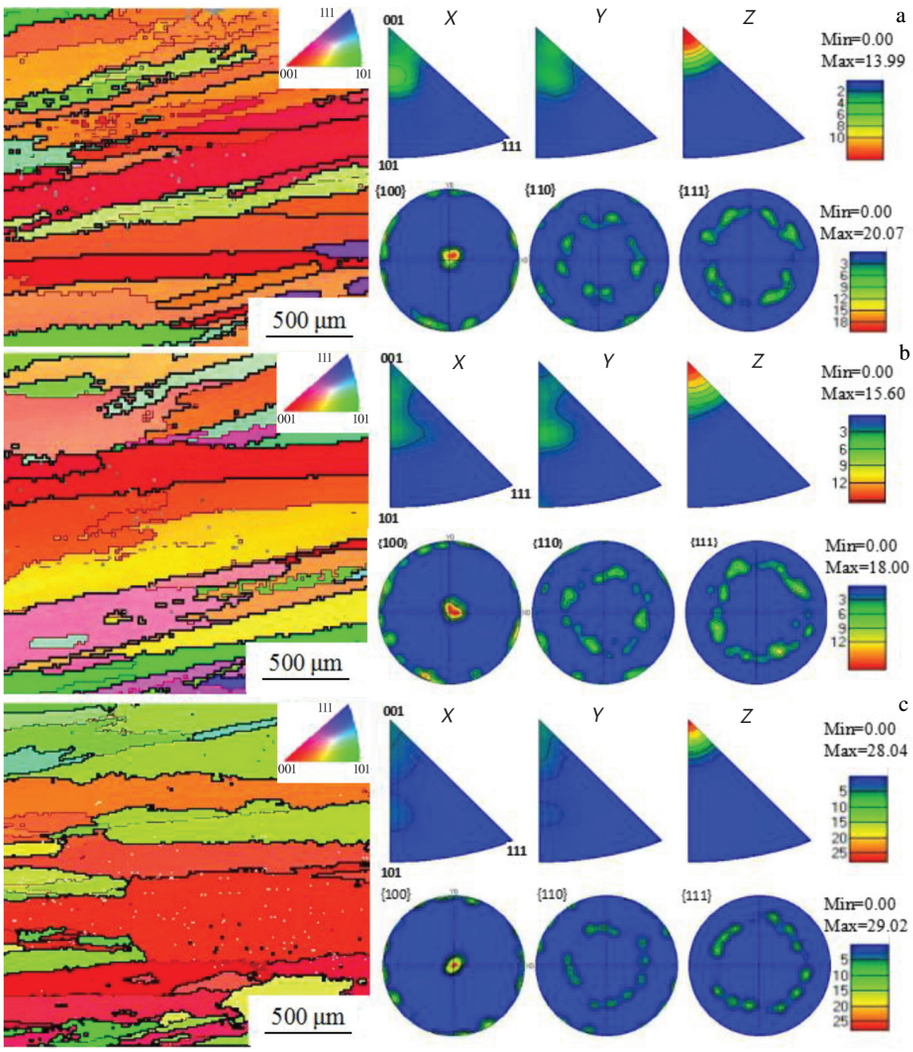

Fig.5 IPFs, reverse pole figures, and pole figures of Area 1 (a), Area 2 (b), and Area 3 (c) in overlay welding layer of EQ309L stainless steel

determined by the competitive growth. In the solidification process of welded metal, the grains tend to grow along the direction perpendicular to the boundary of the molten pool, because of larger temperature gradient and the faster heat dissipation along that direction. However, the columnar crystal in each grain tends to grow along the preferred growth direction. For fcc materials, <100> direction is a preferred easy growth direction. Therefore, during solidification, the grain growth direction is roughly perpendicular to the boundary of weld pool, leading to the fact that these grains can grow more easily. The grain growth along other orientations is hindered, as shown in Fig. 5. This competitive growth mechanism determines the grain structure of the welded metal.

2.3 Microstructure analysis of Q345R base metal layer

The heat-affected zone of overlay welding layer is about 9 mm in width, and the interface structure of Q345R stainless steel of 7~8 mm away from the overlay welding layer is shown in Fig.6. Q345R base metal basically occupies the blue recrystallized area, indicating that most grains are recrystallized and some of them are in the status of recrystallization recovery. The average grain size is 20~25 μm, the degree of internal distortion of these grains is greatly reduced, and the average grain orientation is 30.5°. However, the original RD and band-like traces of grains can still be observed.

The interface structure of Q345R stainless steel of 15 mm away from the overlay welding layer is shown in Fig. 7. As shown in Fig.7b, Q345R base metal basically occupies the red deformed area with an average grain orientation of 7° , suggesting that most grains suffer serious internal distortion and have a large number of dislocations. The original RD and the band-like traces can be clearly discovered. The yellow area in Fig.7 indicates that the reversion occurs.

3 Discussion

3.1 Element analysis of interface

Fig. 8 shows the distribution of alloying elements at the bonding interface. It can be clearly observed from the line scanning results that Cr, Fe, and Ni are diffused in both sides of the bonding interface, and their diffusion distances are 40~50 μm. The obvious diffusion phenomena can be observed

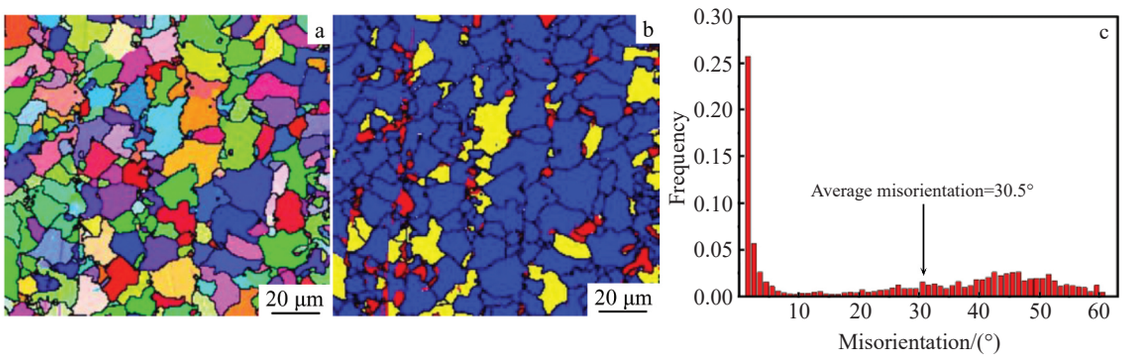

Fig.6 IPF (a), recrystallization figure (b), and misorientation distribution of grain boundaries (c) of Q345R base metal near the fine-grain region

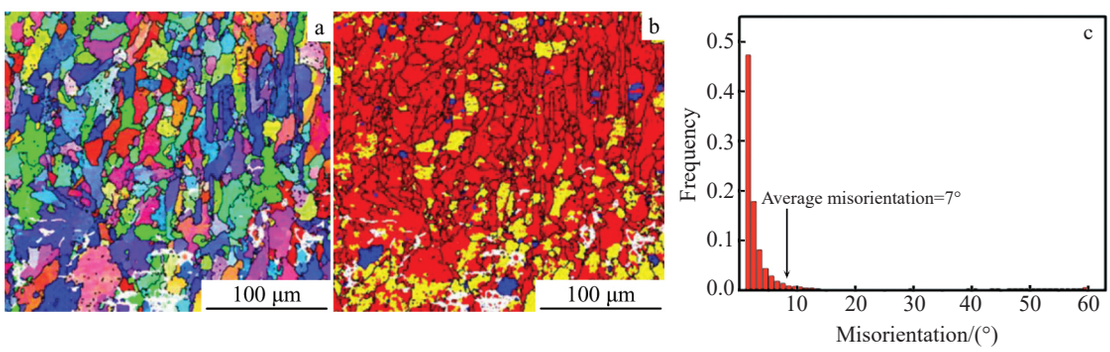

Fig.7 IPF (a), recrystallization figure (b), and misorientation distribution of grain boundaries (c) of Q345R matrix

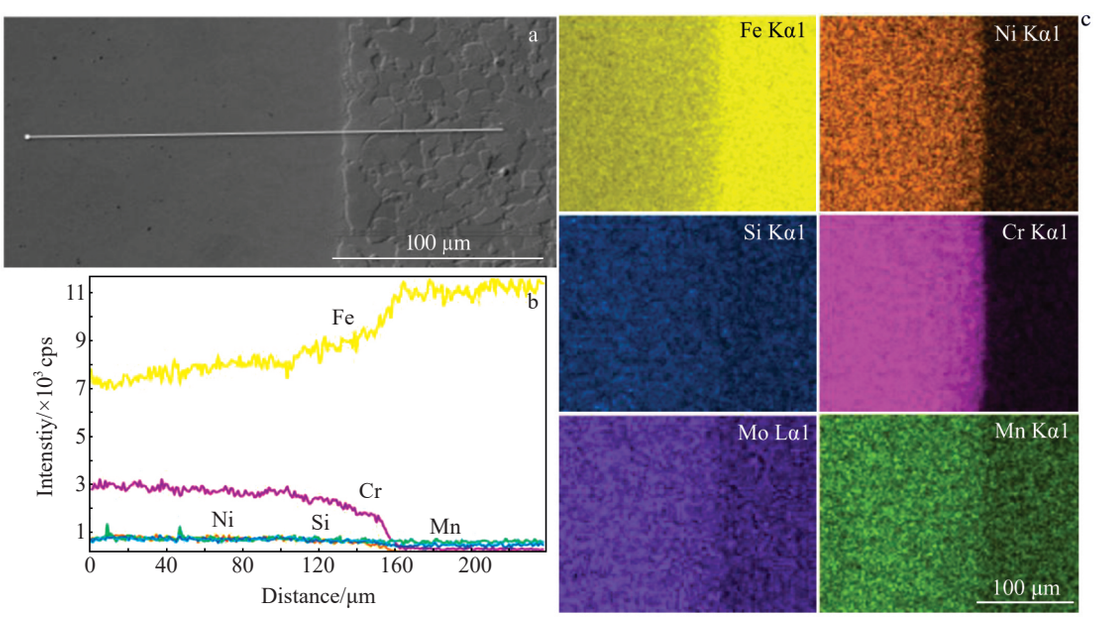

Fig.8 SEM morphology (a), EDS element line scanning along marking line in Fig.8a (b), and element distributions (c) of interface

near the interface for Cr, Fe, and Ni elements. The increase in strength shows important impacts. The interdiffusion of metallic elements can also be revealed on both sides of the interface.

3.2 Microhardness

The microhardness test results are shown in Fig.9. The peak microhardness is achieved at the heat-affected zone, and the microhardness gradually decreases along the EQ309L side and

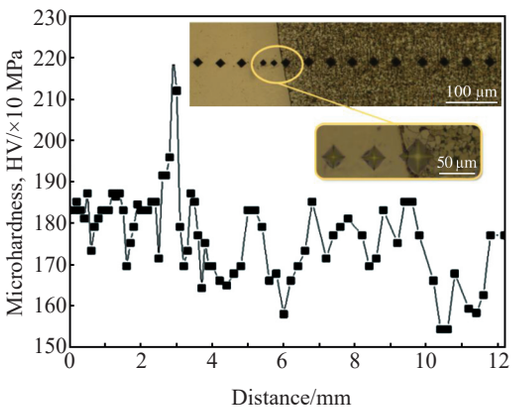

Fig.9 Vickers microhardness distribution and indentation morphology of specimen after band electrode submerged arc overlay welding

along Q345R side, separately. Due to the larger grain size caused by welding and the element diffusion at the interface, the microhardness is greater than that of the base metal, and the maximum microhardness is 2200 MPa. Because the EQ309L welded material consists of austenite, the microhardness is 1700~1850 MPa. The Q345R base metal consists of ferrite and pearlite, and its microhardness is 1550~1850 MPa. The reason for the large fluctuations in the microhardness of the base metal is that the microhardness of ferrite and pearlite is different. The lamellar fine pearlite structure has high microhardness, but its distribution is uneven. The microhardness of base metal, heat-affected zone, and overlay welding layer is less than 2250 MPa but still within a reasonable range, ensuring that the overlay welding layer has good toughness.

3.3 Evolution mechanism

Arc fusion welding technique realizes the metallurgical combination of materials through the solidification and crystallization of the weld pool. Generally, the weld pool has a solidified structure, such as columnar crystals or dendrites. The base metal has a solid structure, and its grain size depends on the heat source. The area between the solidified structure and the solid structure of base metal is the fusion zone. In the actual welding process, different solidification structures appear, including columnar crystals, dendrites, and cellular crystals, due to different temperature gradients and cooling rates. Fig. 10 briefly describes the effect of the temperature gradient on the interface morphology by undercooling and solidification[21]. G_1 and G_2 are the temperature gradients in the liquid phase, d refers to the crystallographic direction of weld grains. A small degree of undercooling is required to solidify the grains and form columnar crystals. When the degree of undercooling is large, the solidified grains are more likely to form dendrites. Ritter et al[22] proposed that the growth rate of each grain is different due to the grain anisotropy, and the grain growth with faster growth rate can inhibit the ones with slow growth rate in the grain solidification and growth. Theoretically, for fcc and bcc materials, including most welded metals or alloy crystals, the preferred growth direction is the crystal direction[21], which agrees well with the competitive growth mechanism, as shown in Fig.10.

Fig. 11 shows the schematic diagram of the microstructure of specimen after band electrode submerged arc overlay welding, according to the results proposed by Kou[21]. Below the fusion line, there are thermally affected coarse-grain regions, fine-grain regions, near fine-grain regions, and matrix. Above the fusion line, there are the fusion zone, epiphytic grain zone, and columnar grain zone. The preferred grain growth direction is <100> because the austenite has fcc structure. Therefore, when the grains grow fast, their growth direction is parallel to the direction of temperature gradient[18], and the grains are regarded as the preferentially oriented grains. With the advancement of the solid-liquid interface, the grains with the preferred <100> orientation grow quickly, thereby hindering the growth of other grains, and stop growing at the beginning of the solidification. In the fusion zone in Fig. 4, the grains along <100> orientation in base

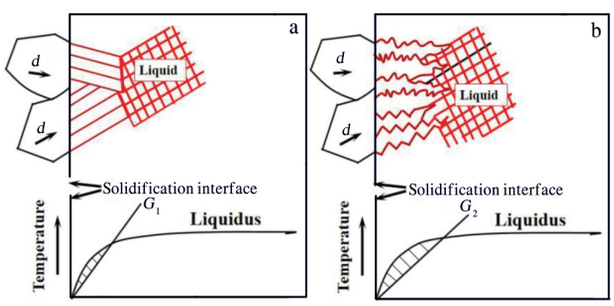

Fig.10 Influence of temperature gradient on interface morphology by undercooling (a) and solidification (b)

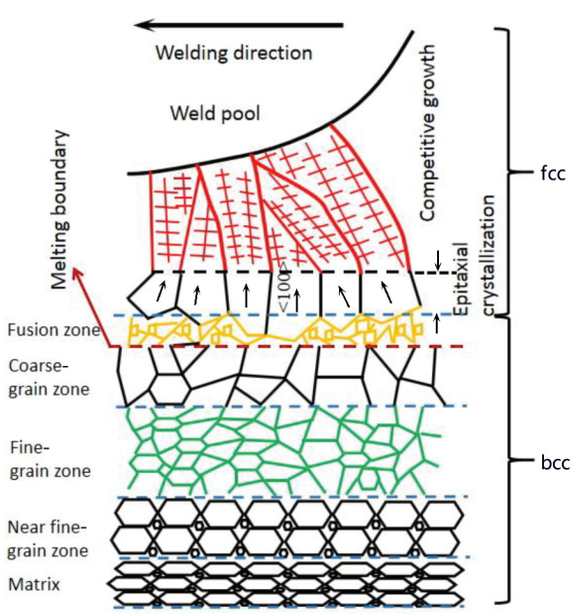

Fig.11 Schematic diagram of microstructure of specimen after band electrode submerged arc overlay welding

metal is greatly increased after solidification, indicating that the solidification growth of welded metal conforms to the competitive growth mechanism.

Owing to the epitaxial growth, the crystalline orientation does not change; the poor orientation of the grain boundaries and the grain orientation of the welded area are mainly affected by the grain orientation of the base metal at the weld pool. Therefore, according to the competitive growth mechanism, the welded grains can grow along with the base metal grains near the fusion zone with <100>//<100> and {100}//{100} as the main orientation relationship. Finally, the <100> texture is formed in the welded area. As shown in IPFs in Fig. 5, the welded grains have obvious <100> texture characteristics.

4 Conclusions

1) Below the fusion line, there are thermally affected coarse-grain regions, fine-grain regions, near fine-grain regions, and matrix. Above the fusion line, there are the fusion zone, epiphytic grain zone, and columnar-grain zone. The preferred grain growth direction is <100> direction. The EQ309L overlay welding layer has coarse grains and columnar crystal morphology with obvious <100> texture characteristics.

2) The transition zone is 35~40 μm away from the fusion line of Q345R matrix with the body-centered cubic structure. In the overheated coarse-grain area, the average grain size of Q345R stainless steel is 30~40 μm, and the grain coarsening phenomenon is not severe. The fine-grain area has an average grain size of 10~20 μm.

3) Most grains in the fine-grain area near Q345R matrix are recrystallized with an average grain size of 20~25 μm. The degree of internal distortion of the grains is greatly reduced, and the average grain orientation is 30.5°. However, the grain strips are band-like along the original rolling direction. Most grains in Q345R matrix are severely distorted with an average grain orientation of 7°.

References

1 Mohammadzadeh R, Akbari A. *Materials Characterization*[J], 2014, 93: 119

2 Hou Zhenguo, Zhang Yanhui, Chen Liyuan *et al*. *Hot Working Technology*[J], 2016, 45(11): 22 (in Chinese)

3 Liu Haixiang, Yang Li, Ge Jinguo. *Hot Working Technology*[J], 2016, 45(3): 242 (in Chinese)

4 Zhang Maolong, Lu Yanhong, Chen Shenghu *et al*. *Acta Metallurgica Sinica*[J], 2020, 56(8): 1057 (in Chinese)

5 Xiong Q, Li H J, Lu Z P *et al*. *Journal of Nuclear Materials*[J], 2018, 498: 227

6 Lai Qianshang, Jiang Yanzhong. *Electric Welding Machine*[J], 2009, 39(8): 9 (in Chinese)

7 Gallazi G, Rigoal S, Kubenka M. *Electric Welding Machine*[J], 2010, 40(8): 5

8 Liu Yang, Wang Lei, Song Xiu *et al*. *Proceedings of the International Conference on Theoretical, Applied and Experimental Mechanics*[C]. Corfu: Springer, 2019, 13: 48

9 Liu Yang, Wang Lei, Song Xiu *et al*. *Acta Metallurgica Sinica* [J], 2019, 55(9): 1221 (in Chinese)

10 Shi Yu, Zhang Yingying, Guo Xiaoxiao. *Materials for Mechanical Engineering*[J], 2019, 43(10): 20 (in Chinese)

11 Ming Hongliang, Zhang Zhiming, Wang Jianqiu *et al*. *Acta Metallurgica Sinica*[J], 2017, 53(1): 57 (in Chinese)

12 Wang H T, Wang G Z, Xuan F Z *et al*. *Engineering Failure Analysis*[J], 2013, 28: 134

13 Wang Haitao, Wang Guozhen, Xuan Fuzhen *et al*. *Nuclear Techniques*[J], 2013, 36(4): 40 628 (in Chinese)

14 Ming H L, Zhu R L, Zhang Z M *et al*. *Materials Science and Engineering A*[J], 2016, 669: 279

15 Wang W, Lu Y H, Ding X F *et al*. *Materials Characterization*[J], 2015, 107: 255

16 Lu Yanhong, Zhang Maolong, Tang Weibao *et al*. *Pressure Vessel Technology*[J], 2017, 34(9): 21 (in Chinese)

17 Wang W, Liu T G, Cao X Y *et al*. *Materials Characterization*[J], 2017, 132: 169

18 Kaneko Y, Yamane S, Oshima K. *Welding in the World*[J], 2009, 53(11-12): 333

19 Xie L, Ziegmann G, Jiang B Y. *Journal of Central South University of Technology*[J], 2009, 16(5): 774

20 Nelson T W, Lippold J C, Mills M J. *Science and Technology of Welding and Joining*[J], 1998, 3(5): 249

21 Kou S. *Welding Metallurgy*[M]. Hoboken: John Wiley & Sons, 2003: 180

22 Ritter A M, Savage W F. *Metallurgical Transactions A*[J], 1986, 17(4): 727

带极埋弧堆焊EQ309L不锈钢的微观组织EBSD分析

赵　菲[1]，刘子敬[1]，马立峰[2]，赵广辉[2]

(1. 太原科技大学 材料科学与工程学院，山西 太原 030024)

(2. 太原重型机械教育部工程研究中心，山西 太原 030024)

摘　要：采用带极埋弧堆焊在Q345R基体表面堆焊EQ309L不锈钢焊带。运用电子背散射衍射（EBSD）表征技术，观测了Q345R和EQ309L之间的EQ309L侧、Q345R侧和界面的微观组织特征。结果表明：在Q345R基体上大部分晶粒内部畸变严重，观测到明显的沿原轧制方向的条带状晶粒。在过热粗晶区域，Q345R基体的平均晶粒尺寸为30~40 μm，晶粒粗化不严重；在细晶区，Q345R基体的平均晶粒尺寸为10~20 μm。Q345R基体侧熔合线向堆焊层延伸35~40 μm后的区域是过渡区，该区域具有体心立方（bcc）结构。EQ309L层晶粒粗大，呈柱状晶形貌，具有明显的<100>织构特征。

关键词：微观组织；带极埋弧堆焊；EQ309L；EBSD

作者简介：赵　菲，女，1982年生，博士，副教授，太原科技大学材料科学与工程学院，山西 太原 030024，E-mail：2012020@tyust.edu.cn